

Signatures of dephasing by mirror-symmetry breaking in weak-antilocalization magnetoresistance across the topological transition in $\text{Pb}_{1-x}\text{Sn}_x\text{Se}$

Alexander Kazakov^{1,*}, Wojciech Brzezicki^{1,2}, Timo Hyart^{1,3,†}, Bartłomiej Turowski¹, Jakub Polaczyński¹, Zbigniew Adamus⁴, Marta Aleszkiewicz⁴, Tomasz Wojciechowski¹, Jarosław Z. Domagała⁴, Ondřej Caha⁵, Andrei Varykhalov⁶, Gunther Springholz⁷, Tomasz Wojtowicz¹, Valentine V. Volobuev^{1,8,‡} and Tomasz Dietl^{1,9,§}

¹International Research Centre MagTop, Institute of Physics,

Polish Academy of Sciences, Aleja Lotnikow 32/46, PL-02668 Warsaw, Poland

²Institute of Theoretical Physics, Jagiellonian University, ulica S. Łojasiewicza 11, PL-30348 Kraków, Poland

³Department of Applied Physics, Aalto University, FI-00076 Aalto, Espoo, Finland

⁴Institute of Physics, Polish Academy of Sciences, Aleja Lotnikow 32/46, PL-02668 Warsaw, Poland

⁵Department of Condensed Matter Physics, Faculty of Science,

Masaryk University, Kotlářská 2, Cz-611 37 Brno, Czech Republic

⁶Helmholtz-Zentrum Berlin für Materialien und Energie, Albert-Einstein Strasse 15, D-12489 Berlin, Germany

⁷Institut für Halbleiter- und Festkörperphysik, Johannes Kepler University, Altenbergerstrasse 69, A-4040 Linz, Austria

⁸National Technical University “KhPI”, Kyrpychova Str. 2, 61002 Kharkiv, Ukraine

⁹WPI Advanced Institute for Materials Research, Tohoku University, 2-1-1 Katahira, Aoba-ku, Sendai 980-8577, Japan



(Received 16 January 2021; accepted 18 May 2021; published 16 June 2021)

Many conductors, including recently studied Dirac materials, show saturation of coherence length on decreasing temperature. This surprising phenomenon is assigned to external noise, residual magnetic impurities, or two-level systems specific to noncrystalline solids. Here, by considering the SnTe-class of compounds as an example, we show theoretically that breaking of mirror symmetry deteriorates Berry’s phase quantization, leading to additional dephasing in weak-antilocalization magnetoresistance (WAL-MR). Our experimental studies of WAL-MR corroborate these theoretical expectations in (111) $\text{Pb}_{1-x}\text{Sn}_x\text{Se}$ thin film with Sn contents x corresponding to both topological crystalline insulator and topologically trivial phases. In particular, we find the shortening of the phase coherence length in samples with intentionally broken mirror symmetry. Our results indicate that the classification of quantum transport phenomena into universality classes should encompass, in addition to time-reversal and spin-rotation invariances, spatial symmetries in specific systems.

DOI: [10.1103/PhysRevB.103.245307](https://doi.org/10.1103/PhysRevB.103.245307)

I. INTRODUCTION

One of the most powerful characterizations of quantum systems is in terms of ten universality classes that correspond to different ways fermionic Hamiltonians transform under time-reversal \mathcal{T} , particle-hole, and chiral symmetry operations [1–3]. This generic approach, immune to space symmetry details, allows describing specificities of transport and topological phenomena in a broad range of normal and superconducting materials [1–4]. In the sector of normal conductors, this classification leads to three major experimentally realized cases depending on the presence (+) or the absence (–) of \mathcal{T} and the spin-rotation invariance \mathcal{S} . The instances in the presence of time-reversal symmetry are referred to as orthogonal (++) and symplectic (+–) class, whereas the universality class in the absence of time-reversal symmetry is known as the unitary class [1,5]. The unitary

class is sometimes divided into subclasses depending on the existence of the spin-rotation symmetry and spin polarization in systems where the effects of carrier interactions are relevant [6,7].

It becomes, however, increasingly clear that this picture is not complete. For instance, weak-antilocalization (WAL) magnetoresistance (MR) described by the Hikami-Larkin-Nagaoka (HLN) formula [5] is expected for the symplectic class in the limit of strong spin-orbit scattering, for example, due to: (i) spin-momentum locking of carriers encircling two-dimensional (2D) gapless Dirac cones at surfaces of three-dimensional (3D) topological materials [8–11]; (ii) a large precession frequency in the interfacial Rashba field compared to the inverse momentum relaxation time [12]; and (iii) a strong Elliott-Yafet mechanism due to sizable mixing of spin states in the carrier wave functions [13]. Surprisingly, however, robust WAL MR is also observed for graphene [14]. It has actually been found that because of isospin-momentum locking, the carriers encircling 2D gapless Dirac cones acquire the Berry phase $\varphi = \pi$, which eliminates backscattering and, thus, results in MR that mimics the symplectic case, even though the spin-orbit interaction is negligible. However, in graphene also the space group symmetries are important

*kazakov@magtop.ifpan.edu.pl

†timo.hyart@magtop.ifpan.edu.pl

‡volobuev@magtop.ifpan.edu.pl

§dietl@magtop.ifpan.edu.pl

because both the intervalley scattering and trigonal warping of the cones, which makes momentum \mathbf{p} nonequivalent to $-\mathbf{p}$, suppress the WAL effect [14,15]. Similarly, the theoretical discovery of topological indices associated with crystal point group symmetries [16] showed that the tenfold classification has to be much extended to incorporate a rather abundant family of topological crystalline insulators (TCIs) and superconductors [17]. In particular, it was predicted theoretically [18,19] and confirmed experimentally [20–24] that the mirror-symmetry \mathcal{M} can protect the presence of gapless topological Dirac cones on (001) and (111) surfaces of cubic SnTe-type semiconductors with the inverted band structure.

Here, by taking thin films of cubic SnTe-type semiconductors as an example, we show—combining analytic and numerical approaches developed recently [25]—that the Berry phase for carriers encircling the Fermi loops is quantized to π in these systems once inversion symmetry is broken by, for instance, due to the differences in top and bottom surfaces. This quantization is independent of the Fermi level position with respect to the bulk band gap, and occurs for the band arrangement corresponding to topologically nontrivial and trivial phases accessible in $\text{Pb}_{1-x}\text{Sn}_x\text{Se}$ materials with $x > x_c$ and $x < x_c$, respectively, where $x_c = 0.16$ [26,27]. Our detailed analysis supported by a direct conductance determination indicates that WAL MR in these layers might be affected not only by doping with magnetic impurities, as found previously in a range of materials [28–31], but also by breaking \mathcal{M} .

In order to test these theoretical predictions, we have grown a series of epitaxial (111) $\text{Pb}_{1-x}\text{Sn}_x\text{Se}$ thin films with the Sn content $0 \leq x \leq 0.3$ capping *in situ* part of the epilayers by amorphous Se. Angle-resolved photoemission spectroscopy (ARPES) confirms that our samples cover both sides of the topological phase transition. Nevertheless, but in agreement with our theoretical expectations, we observe for any x robust WAL MR, well described by the HLN formula in the limit of strong spin-orbit scattering and with the prefactor $\alpha = -1/2$ [5]. This insight elucidates why robust WAL MR has previously been observed not only for topological SnTe epilayers [31–34] or $\text{Pb}_{0.7}\text{Sn}_{0.3}\text{Se}$ quantum wells [35], but also for nontopological $\text{PbTe}/(\text{Pb},\text{Eu})\text{Te}$ quantum wells [36]. Importantly, our data reveal striking differences between WAL MR in uncapped films compared to samples in which the amorphous Se surface layer intentionally breaks the mirror symmetry. This breaking of \mathcal{M} , relevant as electrons penetrate the cap, has two consequences revealed here experimentally and explained theoretically: (i) $\tau_\phi(T)$ determined from WAL MR saturates below 4 K in the Se covered samples but not in samples without a Se cap; and (ii) the conductance decay with the in-plane magnetic field faster in films covered by Se. Our results, together with those for graphene [14,15], lead to a rather striking conclusion that specific space symmetries can account for an apparent low-temperature saturation of $\tau_\phi(T)$ determined from WAL MR studies. This finding suggests that hidden spatial-symmetry properties, together with decoherence specific to amorphous solids [37], might have often been responsible for a hitherto mysterious low-temperature saturation of $\tau_\phi(T)$ observed in many systems [38], including recently studied Dirac materials [35,39–42].

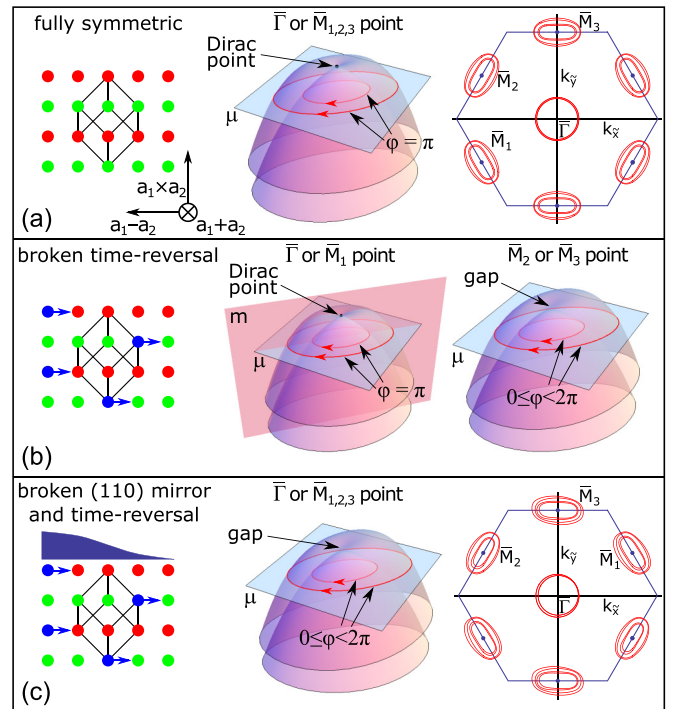


FIG. 1. Dependence of Fermi loops and Berry phases φ on the presence of time-reversal \mathcal{T} and (110) mirror \mathcal{M} symmetries for doped $\text{Pb}_{1-x}\text{Sn}_x\text{Se}$ thin films. (a) If \mathcal{T} and \mathcal{M} are obeyed the Berry phases of the Fermi loops in subbands of a two-dimensional slab are quantized to $\varphi = \pi$, protecting subband crossings at high-symmetry points $\bar{\Gamma}$ and \bar{M}_i (black dot). This also holds when only \mathcal{M} is broken. (b) If \mathcal{T} is broken (e.g., by a Zeeman field shown by arrows) but \mathcal{M} is obeyed the Berry phases are quantized to π only for Fermi loops going around a subbands' crossing at the $\bar{\Gamma}$ and \bar{M}_1 points lying in the mirror plane. (c) The Berry phases are arbitrary when both \mathcal{T} and \mathcal{M} are simultaneously broken (arrows and asymmetric surface layer).

II. THEORY

A. Mirror and time-reversal symmetry protected quantization of the Berry phases

We consider the symmetry-enriched berryology of the (111) multilayer system in the SnTe material class [18] (see the Supplemental Material, Ref. [43] Sec. S1, for more details). By doping the system we obtain Fermi loops around the high-symmetry points $\bar{\Gamma}$ and \bar{M}_i ($i = 1, 2, 3$) (see Fig. 1). The type of doping (electron or hole doping) is not important for our theoretical considerations because both types of doping yield similar Fermi loops and our results follow from generic symmetry arguments. In our calculations, all 2D subbands are nondegenerate along the Fermi loops because of the spin-orbit interaction and the inversion asymmetry due to the presence of inequivalent surfaces. We show that both time-reversal \mathcal{T} and (110) mirror \mathcal{M} symmetries lead to quantization of the Berry phases (see Fig. 2). Due to threefold rotational symmetry, there exists also two other mirror symmetries which would lead to equivalent considerations.

In the presence of time-reversal symmetry obeying $\mathcal{T}^2 = -1$, we obtain that all the Fermi loops have quantized Berry phase $\varphi = \pi$ [see Fig. 1(a)]. To prove this we consider the

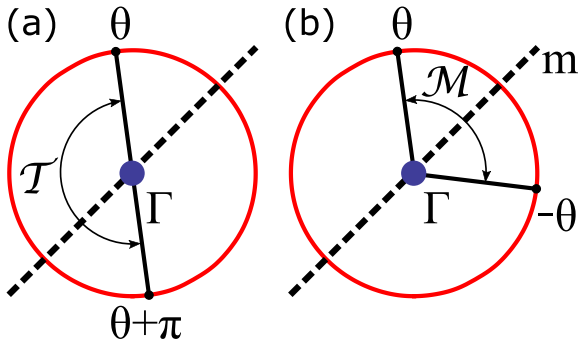


FIG. 2. Action of time-reversal \mathcal{T} and mirror \mathcal{M} symmetries on states belonging to the Fermi loop around $\bar{\Gamma}$ point. Points along the loop are parametrized by the angle θ with respect to the mirror line (dashed). (a) Time-reversal maps state $|\psi_{\theta}^{(n)}\rangle$ onto $|\psi_{\theta+\pi}^{(n)}\rangle$. (b) Mirror symmetry maps state $|\psi_{\theta}^{(n)}\rangle$ onto $|\psi_{-\theta}^{(n)}\rangle$.

eigenstates $|\psi_{\theta}^{(n)}\rangle$, $\theta \in [-\pi, \pi)$, belonging to the n th energy band forming a Fermi loop around $\bar{\Gamma}$ (or \bar{M}_1) point (see Fig. 2). Since θ is periodic variable $|\psi_{\theta}^{(n)}\rangle$ can acquire a Berry phase by a parallel shift along the loop. The gauge-invariant form of the Berry phase is given by

$$\varphi_n = \arg \left[\langle \psi_{-\pi}^{(n)} | \psi_{-\pi+\delta\theta}^{(n)} \rangle \langle \psi_{-\pi+\delta\theta}^{(n)} | \psi_{-\pi+2\delta\theta}^{(n)} \rangle \cdots \times \langle \psi_{\pi-2\delta\theta}^{(n)} | \psi_{\pi-\delta\theta}^{(n)} \rangle \langle \psi_{\pi-\delta\theta}^{(n)} | \psi_{\pi}^{(n)} \rangle \right], \quad (1)$$

where $\delta\theta$ is an infinitesimal step in angle θ . In the presence of a time-reversal symmetry we obtain the states $|\psi_{\theta}^{(n)}\rangle$ for $-\pi \leq \theta < 0$ by diagonalizing the Hamiltonian and we define $0 \leq \theta < \pi$ states as $|\psi_{\theta+\pi}^{(n)}\rangle = \mathcal{T}|\psi_{\theta}^{(n)}\rangle$. By this construction we find that most of the phases in Eq. (1) cancel and we are left with (see Ref. [43], Sec. S2)

$$\varphi_n = \arg \left[- |\langle \psi_{-\delta\theta}^{(n)} | \psi_0^{(n)} \rangle|^2 \right] = \pi. \quad (2)$$

Hence, in the presence of time-reversal symmetry satisfying $\mathcal{T}^2 = -1$ the Berry phases are quantized to π . Equivalently we can say that the Berry phases are equal to π because each Fermi loop encircles a crossing (i.e., Dirac point) of the subbands protected by Kramers degeneracy at high-symmetry points of the Brillouin zone (BZ). We point out that for time-reversal symmetry obeying $\mathcal{T}^2 = 1$ (no spin-orbit interaction) the Berry phases would be quantized to 0. Thus, our symmetry analysis of the Berry phases reproduces the well-known result that materials with strong (weak) spin-orbit coupling support WAL (WL) due to belonging to the symplectic (orthogonal) universality classes [1,5]. This result holds both in the topologically trivial and nontrivial regimes, and therefore we expect WAL independently of the Sn content in $\text{Pb}_{1-x}\text{Sn}_x\text{Se}$ thin films.

It turns out that the presence of crystalline mirror-symmetry \mathcal{M} can lead to the quantization of Berry phases even if time-reversal symmetry \mathcal{T} is broken, e.g., by a nonzero Zeeman field, as shown in Fig. 1(b). Namely, in the presence of mirror symmetry we obtain the states $|\psi_{\theta}^{(n)}\rangle$ for $0 \leq \theta \leq \pi$ by diagonalizing the Hamiltonian and we define $-\pi \leq \theta < 0$ states as $|\psi_{-\theta}^{(n)}\rangle = \mathcal{M}|\psi_{\theta}^{(n)}\rangle$ (see Fig. 2). From Eq. (1) we find that most of the phases cancel due to unitarity of \mathcal{M} and we

obtain (see Ref. [43], Sec. S2)

$$\varphi_n = \arg \left[\langle \psi_{\pi}^{(n)} | \mathcal{M} | \psi_{\pi}^{(n)} \rangle \langle \psi_0^{(n)} | \mathcal{M} | \psi_0^{(n)} \rangle \right], \quad (3)$$

where $|\psi_0^{(n)}\rangle$ and $|\psi_{\pi}^{(n)}\rangle$ are eigenstates of \mathcal{M} with eigenvalues ± 1 . Thus the product under arg function is either +1 or -1, and hence the Berry phases for all mirror-symmetric Fermi loops are quantized to 0 or π [Fig. 1(b)]. Again, we find that $\varphi = \pi$ if the Fermi loop encloses a Dirac point, i.e., a crossing of subbands. For weakly broken \mathcal{T} the crossings stay inside Fermi loops within the mirror plane. However, the Berry phase changes to 0 when they move outside at a topological phase transition for strongly broken \mathcal{T} (see Ref. [43], Sec. S3).

Finally, we find that the Berry phases are arbitrary when both \mathcal{T} and \mathcal{M} are simultaneously broken [Fig. 1(c)]. We emphasize that this symmetry analysis is completely generic, but we have also confirmed these findings by explicitly calculating the Berry phases in the presence of specific perturbations breaking of \mathcal{T} and \mathcal{M} independently of each other (see Ref. [43], Sec. S3).

This theoretical analysis leads to two important predictions that can be directly tested experimentally. First, we obtain a similar behavior of the Berry phases for both topologically nontrivial and trivial materials. We expect that similar WAL-like behavior is observed in $\text{Pb}_{1-x}\text{Sn}_x\text{Se}$ alloys independently of the Sn content. Second, in realistic condensed matter systems, both \mathcal{T} and \mathcal{M} symmetries are always weakly broken. Therefore, the deviations of the Berry phases from the quantized values can be increased by intentionally breaking the \mathcal{T} and \mathcal{M} symmetries more strongly. The crystalline mirror symmetry can be broken in a controllable way by covering the surface of the sample with a suitable material. Amorphous solids have short-range order in the sense that the distances between neighboring atoms are similar to those in the crystal, but the translational symmetry is absent, so that there is no long-range order and all point group symmetries are violated in crystallographic sense (the symmetry operation will not result in the same structure). Therefore, the importance of the crystalline mirror symmetry on the WAL effect can be tested, for instance, by proximitizing the sample with an amorphous semiconductor.

We have confirmed both of these predictions experimentally. However, before discussing our experimental findings, we will next calculate the quantum correction to the conductivity coming from the Cooperon propagator.

B. Quantum correction to the conductivity

In the vicinity of the band crossings appearing at the high-symmetry points we derive a low-energy 2D Hamiltonian for a single pair of subbands in a form of

$$H_{\vec{k},\bar{\sigma}} = \frac{\hbar^2}{2m_e} \vec{k}^2 + \alpha_{\text{so}}(\sigma_x k_y - \sigma_y k_x) + g\sigma_z. \quad (4)$$

Here m_e is the effective mass of the electron; α_{so} is an effective spin-orbit-like coupling that arises from breaking of the inversion symmetry, which is always present due to the surface in these samples but may be too small to be seen by ARPES; g is the mass term induced by the breaking of the mirror symmetry and weak breaking of the time-reversal symmetry; and σ is an

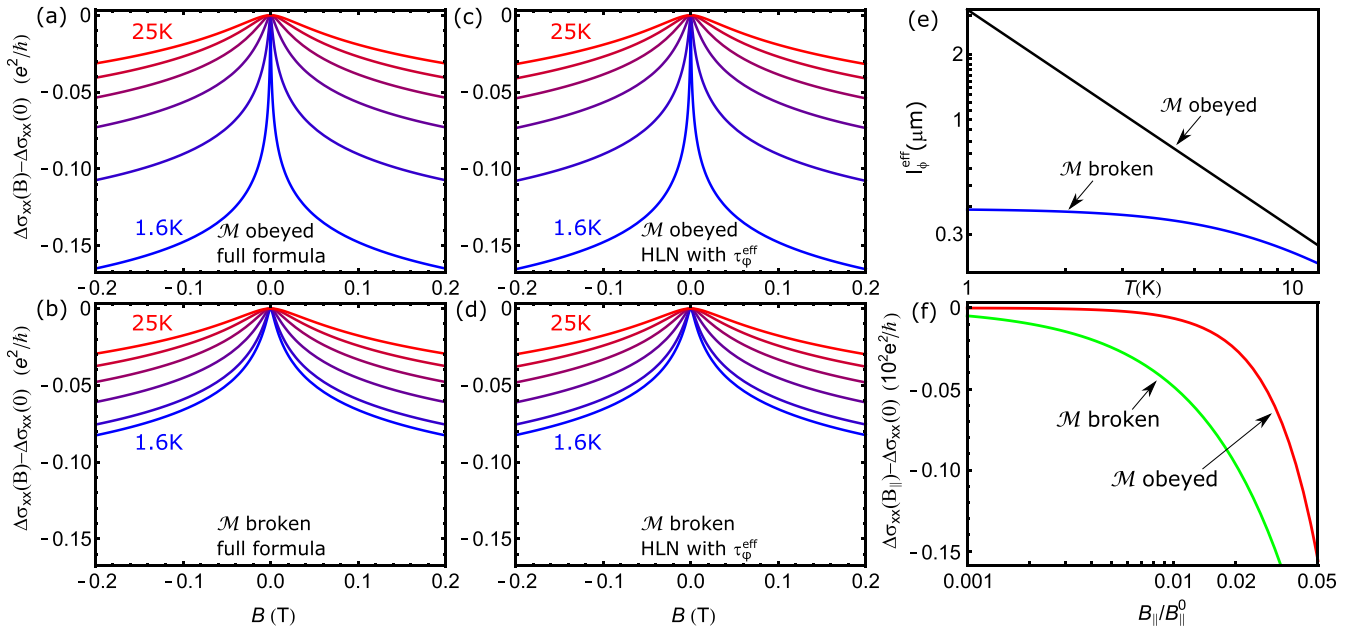


FIG. 3. (a)–(d) $\Delta\sigma_{xx}$ as a function B in the fully symmetric and symmetry-broken cases for temperatures $T = 1.6, 5, 10, 15, 20, 25$ K. (a) and (b) Numerically calculated quantum correction to the conductivity. (c) and (d) $\Delta\sigma_{xx}$ calculated from the modified HLN formula (10) employing the effective dephasing time τ_{ϕ}^{eff} [Eq. (11)]. (e) Effective dephasing length $l_{\phi}^{\text{eff}} = (D_e \tau_{\phi}^{\text{eff}})^{1/2}$ as function of temperature for fully symmetric and symmetry-broken cases. (f) $\Delta\sigma_{xx}$ as a function of the in-plane field $B_{||}$ in the fully symmetric and symmetry-broken cases.

effective pseudospin variable which describes entangled spin and orbital degrees of freedom.

The quantum correction to the conductivity can be written as [44]

$$\Delta\sigma_{xx} = -\frac{e^2 D_e}{\pi \hbar L^2} \sum_{\vec{Q}} \sum_{\alpha, \beta = \pm} C_{\alpha\beta\beta\alpha}(\vec{Q}), \quad (5)$$

where $D_e = v_F l / 2$ is the 2D diffusion constant, $l = v_F \tau$ is the elastic mean-free path, v_F is the Fermi velocity, τ is the elastic scattering time, L^2 is the area of the sample, and $\alpha, \beta = \pm$ are the pseudospin indices of the Cooperon propagator C . For weak disorder ($\tau E_F / \hbar \gg 1$ where E_F is the Fermi energy) the Cooperon propagator can be approximated as

$$C(\vec{Q}) = \tau \left(1 - \int \frac{d\Omega}{2\pi} \frac{1}{1 - i\tau \Sigma(\hbar)} \right)^{-1}, \quad (6)$$

where

$$\Sigma(\vec{Q}) = H_{\vec{Q}-\vec{k}, \vec{\sigma}'} - H_{\vec{k}, \vec{\sigma}} \quad (7)$$

is a 4×4 matrix describing two interfering electrons with pseudospins $\vec{\sigma}'$ and $\vec{\sigma}$. The integral in Eq. (6) is over all angles of velocity $\vec{v} = \hbar \vec{k} / m_e$ on the Fermi surface. By taking lowest order terms in \vec{Q} and α_{so} , we can write the quantum correction to the conductivity in the absence of the magnetic field as

$$\Delta\sigma_{xx} = \frac{e^2}{\pi \hbar L^2} \sum_{\vec{Q}} \text{Tr} \left[\Gamma \left(\frac{1}{D_e \tau_{\phi}} + H_c \right)^{-1} \right], \quad (8)$$

where H_c is a non-Hermitian Cooperon Hamiltonian

$$H_c = \vec{Q}^2 + 2Q_{so} \vec{Q} \cdot \hat{a} \vec{s} + Q_{so}^2 (S_x^2 + S_y^2) - i \frac{g}{\hbar D_e} (\sigma'_z - \sigma_z), \quad (9)$$

$Q_{so} = 2m_e \alpha_{so} / \hbar^2$ and τ_{ϕ} is the dephasing time. Singlet and triplet interference is encoded in matrix Γ having three -1 eigenvalues in the $\sigma\sigma'$ triplet sector and $+1$ in the singlet sector. The perpendicular magnetic field can be introduced in the Cooperon Hamiltonian by minimal substitution $\vec{Q} \rightarrow \vec{Q} + 2e\vec{A}/\hbar$, and the summation in this case should be taken over the Landau levels (see Ref. [43], Sec. S4 for details).

The parameter $g = 0$ unless both time-reversal and mirror symmetry are simultaneously broken (see Ref. [43], Sec. S4 for details). We can assume that the time-reversal symmetry is always weakly broken by the same amount due to the intrinsic mechanisms, but the breaking of the mirror symmetry is tunable and depends on how the sample is covered. Thus, in uncovered samples we assume that $g \approx 0$ but in the presence of the cover which breaks the mirror symmetry g becomes significantly larger and we assume that it is given by $g = 1.75$ meV. Note that the gap opened by g is still too small to be observed by ARPES, but the WAL measurement is a very sensitive probe of the symmetry-breaking field, so that already such a small value of g can dramatically show up in the transport experiments: The resulting dependencies of $\Delta\sigma_{xx}$ on B , in the fully symmetric and symmetry-broken cases, are shown in Figs. 3(a) and 3(b) (lines labeled $T = 1.6$ K). In this calculation we have used the parameters: $v_F = 7.3 \times 10^5$ m/s, $l = v_F \tau = 20$ nm, and $l_{\phi} = (D_e \tau_{\phi})^{1/2} = 2$ μm at 1.6 K. (In general the phase-coherence length depends on temperature, as discussed below, and therefore we fix here the phase-coherence length at temperature $T = 1.6$ K.) Moreover, we have estimated that $Q_{so} = 1.022 \times 10^8 \text{m}^{-1}$, so that the pseudospin precession length is $l_{so} = 2\pi / Q_{so} \approx 60$ nm (see Ref. [43], Sec. S4 for details).

The breaking of mirror and time-reversal symmetries by the symmetry-breaking field g leads to an opening of a small

energy gap at the band crossings and to the destruction of the quantization of the Berry phase (see Ref. [43], Sec. S4 for details). Due to the latter reason, the symmetry-breaking field randomizes the phases of the backscattering paths destroying their systematic destructive interference that was caused by the quantization of the Berry phase to $\varphi = \pi$. Therefore, in the presence of the symmetry-breaking field g there is a new length scale which limits the increase of the WAL effect with lowering temperature (see Fig. 3). Although the symmetry-breaking field is a quantum-coherent effect the qualitative picture discussed above suggests that it has a similar effect as phase breaking phenomena described by l_ϕ . We have confirmed this expectation by demonstrating (see Fig. 3) that the conductivity calculated from the full expression can be reproduced by a modified HLN formula given by

$$\begin{aligned} \Delta\sigma_{xx}(B) - \Delta\sigma_{xx}(0) &= \frac{-e^2}{4\pi^2\hbar} \left[\psi \left(\frac{1}{2} + \frac{1}{4\tau_\phi^{\text{eff}} B} \frac{\hbar}{eD_e} \right) - \log \left(\frac{1}{4\tau_\phi^{\text{eff}} B} \frac{\hbar}{eD_e} \right) \right], \end{aligned} \quad (10)$$

where τ_ϕ^{eff} is an effective dephasing time

$$\tau_\phi^{\text{eff}}(T) = \frac{1}{D_e \left(\frac{1}{l_\phi^2(T)} + \frac{1}{l_g^2} \right)} \quad (11)$$

and l_g is the new length scale related with the symmetry breaking field g ,

$$l_g = 2\pi \sqrt{\frac{D_e \hbar}{\sqrt{2}g}}. \quad (12)$$

Thus, if the conductivity is measured as a function of perpendicular magnetic field, the symmetry-breaking field shows up as an effective dephasing length as $l_\phi^{\text{eff}} = (D_e \tau_\phi^{\text{eff}})^{1/2}$, which saturates at low temperatures to l_g . Additionally, to describe the full temperature dependence observed experimentally, we assume that dephasing length depends on temperature as $l_\phi(T) = l_\phi(T_0)T_0/T$. The full temperature dependence of the conductivity from $T = 1.6$ to 25 K obtained this way is shown in Figs. 3(a) and 3(b) both in the absence and presence of the symmetry-breaking field. The corresponding temperature dependencies of the effective dephasing lengths l_ϕ^{eff} are shown in Fig. 3(e). In the absence of the symmetry-breaking field, l_ϕ^{eff} continues to increase at low temperatures, whereas in the presence of the symmetry-breaking field, l_ϕ^{eff} saturates to l_g at low temperatures. Although the symmetry-breaking field g is small, it results in a decrease of l_ϕ^{eff} by almost an order of magnitude at $T = 1.6$ K demonstrating that the effect mirror-symmetry breaking is expected to have dramatic experimental consequences.

Within the low-energy theory the effect of the in-plane field B_{\parallel} (breaking both mirror and time-reversal symmetries) is that it increases the symmetry-breaking field g so that we can write the low-energy Hamiltonian (4) with $g \rightarrow (g + g^* \mu_B |B_{\parallel}|) \sigma_z$. The important scale of the in-plane magnetic field is therefore $B_{\parallel}^0 = g/g^* \mu_B$, where the symmetry-breaking field due to the in-plane field becomes equal to the symmetry breaking field due to the covering of the sample. Then, in the limit of zero perpendicular magnetic field and $T = T_0$ we obtain the result

shown in Fig. 3(f) for $\Delta\sigma_{xx}$. For $|B_{\parallel}| < B_{\parallel}^0$ the conductivity decreases faster in the symmetry-broken case as a function of the in-plane field.

We point out that in this analysis the effect of the in-plane field can also include orbital effects, because also the orbital effects of the in-plane magnetic field break mirror and time-reversal symmetries, and therefore lead effectively to an increase of g in the low-energy theory. Although the explicit dependence of the energy gap on $|B_{\parallel}|$ can be more complicated, the result that the conductivity decreases faster in the symmetry-broken case seems to be relatively robust if the applied in-plane field is reasonably small. (For this result the assumption that the gap increases linearly with $|B_{\parallel}|$ is not necessary.) This result is also consistent with analysis based on Berry phases since the increase of the gap leads to larger deviation of the Berry phases from the quantized value.

III. SAMPLES GROWTH, CHARACTERIZATION, AND PROCESSING

We test the theory on (111) $\text{Pb}_{1-x}\text{Sn}_x\text{Se}$ 50-nm-thick films deposited by molecular beam epitaxy (MBE) on freshly cleaved (111) BaF_2 substrates under the base pressure below 10^{-9} mbar. We employ the PREVAC 190 growth chamber equipped with elemental Pb, Sn, and Se sources, whose flux ratio is controlled by a beam flux monitor placed in the substrate position. Typical selenium to metal flux ratio is of the order of 3:2. The structural quality of the film surface is monitored *in situ* by the reflection high-energy electron diffraction (RHEED). The film growth rate determined by pronounced RHEED oscillations is in the range 0.1–0.3 nm/s. *Ex situ* x-ray diffraction (XRD) measurements have been performed by PANalytical X'Pert Pro MRD diffractometer with a 1.6 kW x-ray tube (vertical line focus) with $\text{CuK}\alpha_1$ radiation ($\lambda = 1.5406$ Å), a symmetric $4\times\text{Ge}(220)$ monochromator, and for high resolution measurements a channel-cut $\text{Ge}(220)$ analyzer. Atomic force microscopy (AFM) images have been obtained in tapping mode using a Veeco Nanoscope IIIa microscope. Additional morphological and composition characterization is accomplished by field emission scanning electron microscopy (FE-SEM) with a neon 40-Auriga Carl Zeiss microscope equipped with energy dispersive x-ray spectroscopy (EDX) system QUANTAX 400 Bruker. Growth conditions, namely the ratio of the beam fluxes and growth temperature, have been thoroughly optimized to obtain high quality thin films with Sn content varying from 0 to 0.40.

Two series of films have been prepared to study the influence of both topological transition and break of the mirror symmetry on the WAL phenomena: the first series consists of bare epilayers A–E, while the samples in the second series (epilayers F–J) are covered by a 100-nm-thick amorphous and insulating Se cap. In each series, Sn content is varied to drive part of the films through the topological transition at low temperatures. The amorphous Se cap layer has been confirmed to be insulating in a separately checked Se/ BaF_2 structure. As shown in Ref. [43], Sec. S5, XRD structural analysis of Se covered samples revealed no additional strains compared to the bare epilayers. The Se cap also serves as a protection against contamination for ARPES measurements.

To ensure that the topological transition indeed takes place, the band structure at the surface of G and D epilayers with trivial and nontrivial compositions, respectively, have been characterized by ARPES at UE112 PGM-2a-1² beamline of BESSY II (Berlin) in the photon energy range 15–90 eV and horizontal light polarization using a six-axes automated cryomanipulator and a Scienta R8000 electron spectrometer. Typical energy and angular resolutions are better than 20 meV and 0.5°, respectively.

Figures 4(a)–4(d) present ARPES spectra and the second derivative of ARPES data taken at 12 K with photon energy of 18 eV in the vicinity of the $\bar{\Gamma}$ point. As seen, the results reveal the presence of precursor surface states [45,46] in the film with Sn content corresponding to the trivial case [Pb_{0.94}Sn_{0.06}Se, Figs. 4(a) and 4(c)] and gapless surface states in the topologically nontrivial case [Pb_{0.81}Sn_{0.19}Se, Figs. 4(b) and 4(d)]. As shown in Fig. 4(e), the surface band gaps determined here by ARPES at several temperatures are in good agreement with the ARPES data for bulk samples [20] and the semiempirical Grisar formula [47]. This agreement demonstrates that residual strains detected by XRD have a minor effect on the band structure. At the same time, the Rashba splitting of bands, appreciable in IV–VI semiconductor epilayers under certain growth conditions [48], is not significant.

Grown and characterized epilayers have been further processed for magnetoresistance (MR) measurements to the form of Hall bars by e-beam lithography and Br wet etching with the long arm along a $\langle 110 \rangle$ direction revealed by cleavage of BaF₂, as depicted in Fig. 5(a). The in-plane magnetic field was oriented along the current in the tilted field experiments. Resistivity measurements were performed in an 8 T/1.5 K cryostat, using a standard lock-in technique at 20–30 Hz with the excitation current from 1 μ A down to 10 nA at the lowest temperature. We checked that lowering of current down to 1 nA did not affect positive low-field MR, meaning that the saturation of the phase breaking length at low temperatures we have found in samples covered by Se cannot be explained by Joule heating. Results of resistivity and Hall effect measurements for all studied samples are summarized in Ref. [43], Sec. S6. The carrier mobilities in Se-covered films are typically higher than in the absence of the Se cap, indicating that the deposition of Se does not lead to any kind of reduction of the sample quality.

Despite that ARPES data presented in Figs. 4(a)–4(d) confirm the expected *n*-type character of Pb_{1-x}Sn_xSe, a positive sign of the Hall coefficient is observed, pointing out to a relatively large contribution from holes at the interface to BaF₂, as found earlier for PbTe/BaF₂ epilayers [51]. High-field parabolic positive MR for the field perpendicular to the film plane, shown in Figs. 5(b) and 5(c), is consistent with a multichannel character of charge transport (valleys, 2D subbands, *n*-type, and *p*-type layers), whereas a linear component in the highest field suggests and an admixture of the Hall resistance caused by lateral inhomogeneities [52].

IV. MAGNETORESISTANCE IN WEAK MAGNETIC FIELDS: EXPERIMENT VS THEORY

Interestingly, and crucially for this work, we find the existence of low-field temperature-dependent positive MR in all

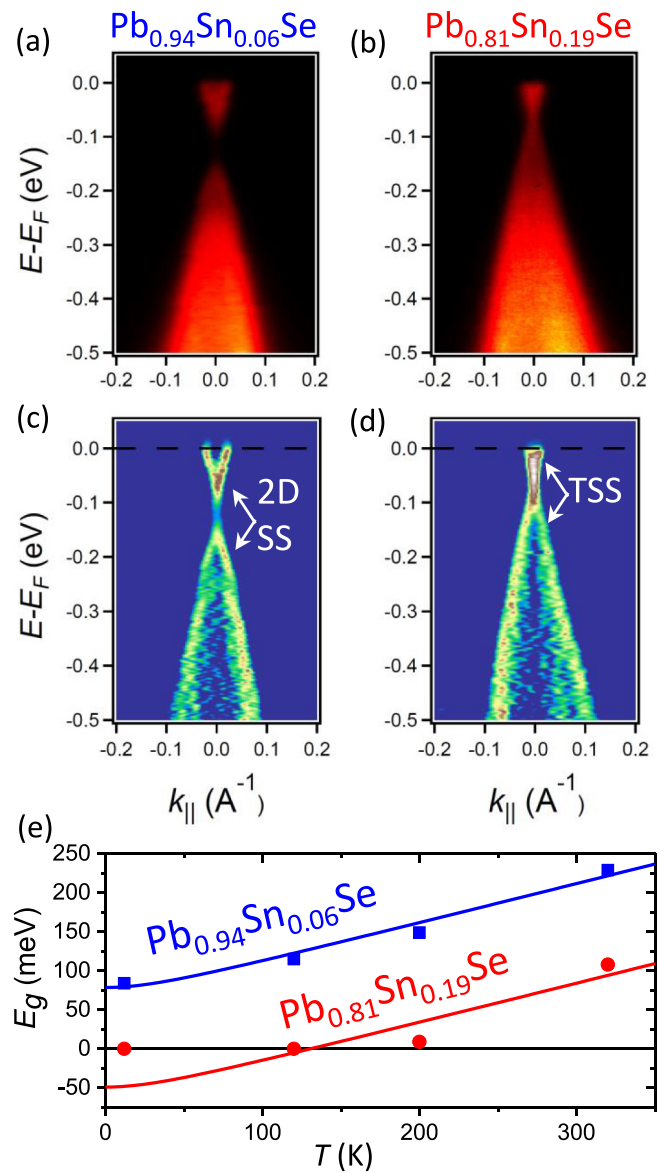


FIG. 4. ARPES results. (a)–(d) Dispersion and corresponding second derivative of ARPES data taken at 12 K with photon energy of 18 eV in the vicinity of the $\bar{\Gamma}$ point. (a) and (c) Results trivial Pb_{0.94}Sn_{0.06}Se (band gap of 84 meV) and (b) and (d) topological Pb_{0.81}Sn_{0.19}Se epilayers (gapless states with Dirac dispersion, as observed previously [24,49,50]). Sample surfaces are *n* type. (c) Second derivative plots confirm the presence of gaped precursor surface states in the trivial phase [45,46]. (e) Surface band gaps measured at several temperatures (points) are well described, above the topological phase transition, by the semiempirical Grisar formula [47] for the bulk band gap (solid lines) thus proving a negligible effect of strains on the band structure of the studied epilayers.

epilayers regardless of their composition. Except for PbSe, this MR dominates only in the diffusive regime $l \ll l_B$, where l is the mean-free path and l_B is the magnetic length. According to the theory developed here, we assign this MR to the Berry phase quantization brought about by symmetries rather than by a nontrivial character of the topological phase. In particular, the mirror symmetry leads to WAL even if time-reversal symmetry is slightly broken. Within this scenario,

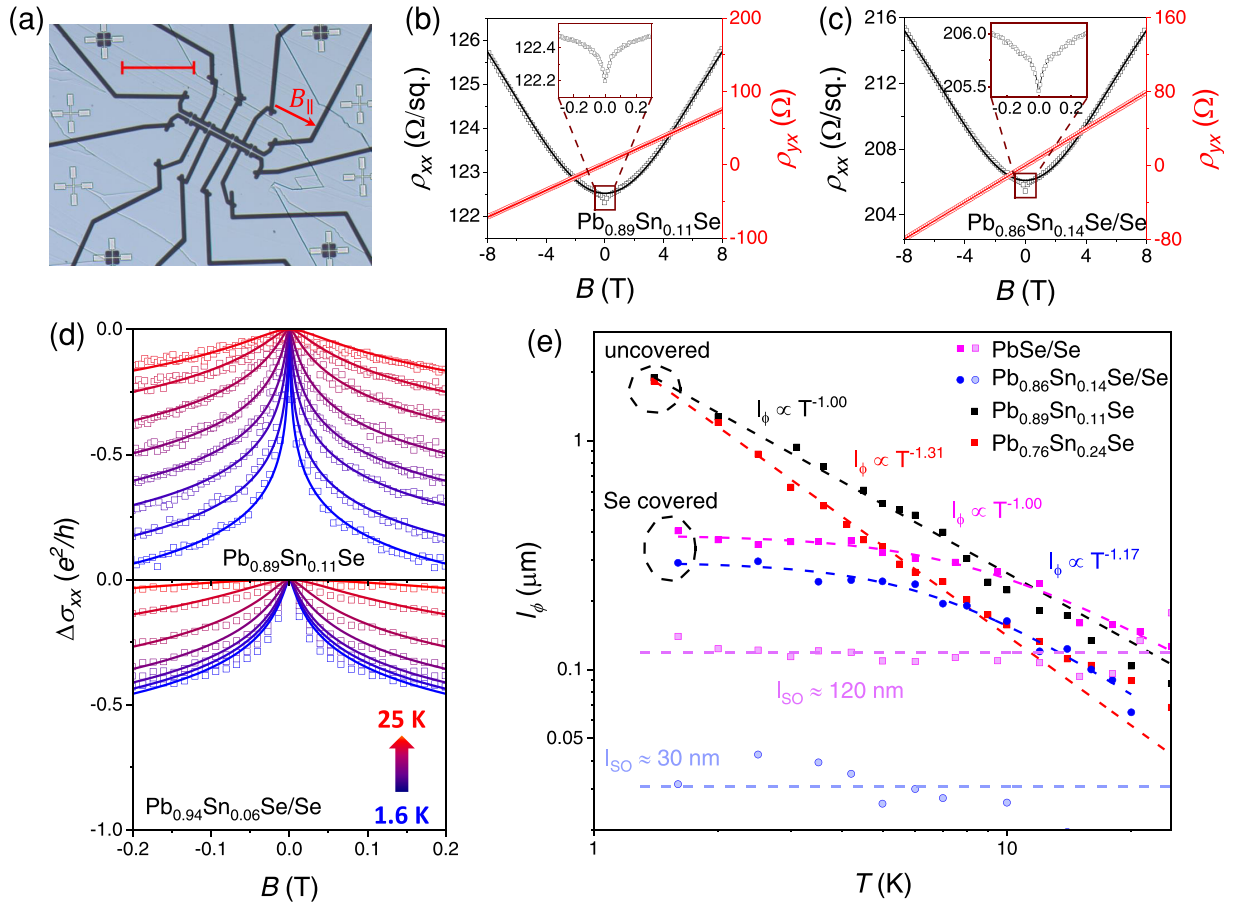


FIG. 5. Determination of the phase coherence length $l_\phi(T)$ from MR data in the magnetic field perpendicular to the epilayer plane. (a) Photo of a processed Hall-bar (epilayer B, $x_{\text{Sn}} = 0.11$); conducting channel resides on a flat area, avoiding cleavage steps of the BaF_2 substrate (scale bar is $200 \mu\text{m}$). (b) and (c) Longitudinal ρ_{xx} (black symbols) and Hall (red symbols) ρ_{yx} resistivities in high (main figures) and weak fields (insets) in epilayers that are uncovered (b) and covered by Se (c). (d) Evolution of the WAL-like low-field MR with increasing temperature in uncovered (upper panel) and Se covered (lower panel) epilayers. Experimental points (empty squares) are fitted to the one-channel HLN expression in the strong spin-orbit approximation (solid lines) treating $l_\phi(T)$ as an adjustable parameter. (e) Determined values of $l_\phi(T)$ in epilayers uncovered by Se increase down to 1.5 K (black and red), while in Se covered epilayers $l_\phi(T)$ saturates at lower temperatures (blue and magenta). Typical values of $l_{\text{so}}(T)$ obtained from the full HLN expression, Ref. [43], Sec. S7.

and by noting that we expect the phase coherence length l_ϕ to be greater than the film thickness $d = 50 \text{ nm}$, the MR is described by the HLN theory in the limit $l_\phi \gg l_{\text{so}}$, where l_{so} is the spin diffusion length limited by spin-orbit interactions, corresponding to the HLN prefactor $\alpha = -1/2$ [5], as given in Eq. (10) for $l_g \rightarrow \infty$. In our case, as shown in Fig. 5(d) and in the Supplemental Material Fig. S8 [43] for the full set of the films, magnetoconductance for all epilayers can be fitted by the one-channel formula, treating $l_\phi(T)$ as the only fitting parameter. This means that l_ϕ is longer than length scales characterizing scattering between subbands and valleys (including surface ones in the topological case) [9,53] as well as between n - and p -type layers. Alternatively, and more probably, because of short length scales characterizing the p -type region, the corresponding WAL or WL MR is shifted to a high field region, so the low field features are solely due to electrons residing closer to the outer surface. It is important recalling that if only one of the parallel layers shows MR, the one channel formula remains valid [9]. As shown in Ref. [43], Sec. S7, by fitting the magnetoconductance data

to the full HLN formula we find $l_{\text{so}} \approx l$, which substantiates our conjecture that in our case WAL MR stems from the Berry phase quantization, and not from a sequence of spin rotations in a varying spin-orbit field resulting in $l_{\text{so}} \gg l$. For comparison we collected in Ref. [43], Sec. S8 the values of $l_\phi(T)$ determined previously for various topological insulators and topological crystalline insulators, the latter data are similar to our results on the both sides of the topological phase transition.

While there is not much difference in WAL MR for samples with Sn content x corresponding to different topological phases, our data reveal a striking dissimilarity in the temperature dependence of magnetoconductance in samples covered and uncovered by Se layers, as shown in Figs. 5(d) and S8 [43]. It is expected that covering of the films by a Se cap may alter the Fermi level position and, thus, change a relative occupancy of electron valleys and subbands in the surface region. However, previous gating experiments on WAL in 2D systems have not indicated any effects of the Fermi level shift on the temperature dependence of the coherence

length. In Sec. III we have discussed precautions undertaken in order to eliminate Joule heating of carriers. Furthermore, unintentional magnetic doping cannot be responsible for the difference between capped and uncapped samples because both types of epilayers have been grown in the same MBE chamber. Relatively large Hall bar dimensions (10–100 μm) exclude finite size effects. Furthermore, as shown in Ref. [43], Sec. S7, fitting to the full HLN expression, i.e., containing l_{so} and the mean-free path l explicitly, confirms that $l_{\text{so}} \approx l \ll l_{\phi}$ [Fig. 5(e)], which rules out a crossover from WAL to WL. Therefore, we assume that the dependence of the WAL magnitude on temperature and the perpendicular magnetic field shown in Fig. 5(d) is solely determined by processes deviating the Berry phase from π , and controlling the magnitude of l_{ϕ} . In the samples without Se layers, $l_{\phi}(T)$ follows the power-law $T^{-p/2}$, with p ranging from 1.4 to 2.6, which corresponds to electron-phonon dephasing mechanism, without any tendency to saturation down to 1.5 K [Fig. 5(e)]. By contrast, in the Se covered epilayers $l_{\phi}(T)$ tends to saturate at temperatures below ≈ 5 K. We have fitted $l_{\phi}(T)$ in Se covered epilayers with $(A_0 + A_1 T^p)^{-1/2}$, which results in the similar values for p , ranging from 1.8 to 2.8 with $l_{\phi}(1.5 \text{ K}) \approx 1\text{--}2 \mu\text{m}$ and 150–400 nm in uncovered and Se covered samples, respectively.

Actually, these striking findings provide a strong support to the theory proposed here [cf. Figs. 3(a)–3(e) and Figs. 5(d)–5(e)]. At high temperature, WAL is still governed by the thermally suppressed l_{ϕ} even if time-reversal symmetry is weakly broken. In bare epilayers, WAL is protected by the quantized Berry phase $\varphi = \pi$ due to the \mathcal{M} , thus l_{ϕ} continues to increase with cooling down. In Se capped epilayers there is a different situation: long interference paths, which are relevant for large values of l_{ϕ} , do not contribute to WAL, since scattering between states at the Fermi level, allowed by mirror-symmetry breaking, randomizes the wave function phase ϕ and average it to zero. At the same time, we assume that the mirror-symmetry breaking by an amorphous cap is stronger than by impurities and defects in high quality crystalline films. Thus, there is a new length scale l_g given in Eq. (12) in the Se-covered films, which limits an increase of WAL MR with lowering the temperature, similarly to the effect of spin-disorder scattering and Zeeman splitting considered previously [5,54,55].

The theory developed here shows explicitly that the application of the in-plane Zeeman field $\vec{h} = g^* \mu_B \vec{B}/2$ leads to a stronger deviation of the Berry phase from the quantized value $\varphi = \pi$ and larger change of conductivity, if reflection symmetry is violated, as shown in Fig. 3(f). In order to test this prediction, we have carried out MR measurements for the magnetic field parallel to the film plane, as in this configuration the role of time-symmetry breaking by the vector potential is reduced [56–58], making the Zeeman effect more important, particularly considering a relatively large magnitude of the electron Landé factor $g^* = 35 \pm 5$ for electrons in PbSe [59]. Since also in the parallel configuration [56–58] and in the presence of the Zeeman effect [54,60,61] the WAL magnitude is controlled τ_{ϕ} in weak magnetic fields, we present in Fig. 6 MR as a function of B/B_{ϕ} , where $B_{\phi} = \hbar/4el_{\phi}^2$. As seen, MR is systematically stronger in samples

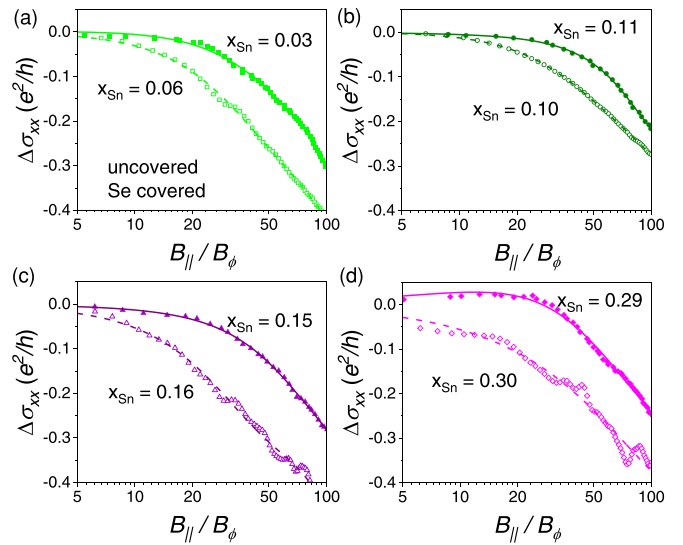


FIG. 6. Effect of mirror-symmetry breaking on MR for magnetic field applied parallel to the film plane. Comparison of MR measured at 4.2 K in the field parallel to the film plane (for which the Zeeman field gives a substantial contribution) for uncovered (full symbols, solid lines) and Se-covered (open symbols, dashed lines) samples with similar x_{Sn} (lines are a guide for the eye); see Ref. [43], Sec. S9 for fitting results obtained employing various formulas for MR in parallel fields $B_{\phi} = \hbar/4el_{\phi}^2$.

covered by the Se cap, in agreement with the theoretical expectations.

V. SUMMARY AND OUTLOOK

Our theoretical results have demonstrated, taking thin films of SnTe class of materials as an example, that the inversion asymmetry and mirror symmetry, rather than the topological phase, are essential for the Berry phase quantization to π and, hence, to the appearance of the robust WAL MR. This implies the existence of the hitherto overlooked length scale in quantum coherence phenomena. This new length is associated with the crystal symmetry breaking rather than with a topological phase transition or with the violation of time-reversal or spin-rotation symmetries considered so far. This offers new prospects in controlling carrier quantum transport by system architectures.

These theoretical expectations have been verified by MR studies on a series of $\text{Pb}_{1-x}\text{Sn}_x\text{Se}$ epilayers, which have revealed the existence of WAL MR on the both sides of topological phase transitions as well pointed out to striking differences in the dependencies of WAL MR on temperature and the magnetic field for samples with the mirror symmetry maintained compared to the films in which mirror symmetry is intentionally broken, as the electron penetration length into the thick amorphous Se layer is longer than into a native surface oxide in uncapped films.

It is certainly appropriate to analyze carefully other mechanisms that could elucidate a strong influence of amorphous Se overlayers on WAL MR. In principle, a reduction of $l_{\phi}(T)$ in Se covered samples might be explained by additional decoherence due to the presence of two-level systems in amorphous

solids. However, the corresponding theory [37] suggests that this would not lead to full saturation of $l_\phi(T)$ at low temperatures. Furthermore, according to formulas describing WAL MR in the parallel configuration [56–58], a stronger WAL MR for the in-plane magnetic field might result from effectively greater thickness of samples covered by Se.

A fascinating question then arises to what extent surprising saturations of $\tau_\phi(T)$ at low temperature observed since decades in many systems [38], and most recently in Dirac materials [35,39–42], have been caused by the hidden spatial symmetry breaking, the mechanisms brought into light by our work.

ACKNOWLEDGMENTS

The International Center for Interfacing Magnetism and Superconductivity with Topological Matter MagTop is supported by the Foundation for Polish Science through the IRA Programme co-financed by EU within SG OP (Grant

No. MAB/2017/1). We acknowledge the Helmholtz-Zentrum Berlin for provision of synchrotron radiation beamtime at UE112 PGM-2a-1² of BESSY II under the EU CALIPSO Grant No. 312284. W.B. also acknowledges support by Narodowe Centrum Nauki (NCN, National Science Centre, Poland) Project No. 2019/34/E/ST3/00404. G.S. also acknowledges support by Austrian Science Fund, Projects No. P30960-N27 and No. I 4493-N.

A.K. and W.B. contributed equally to this work. W.B. and T.H. developed the theory with input from T.D. The samples were grown and characterized by x ray by V.V.V. with the assistance of B.T. and J.J.D., respectively. A.K. carried out processing and magnetotransport measurements with the assistance of J.P. and Z.A., respectively. V.V.V., O.C., and G.S., with the help of A.V., performed ARPES measurements. AFM data were collected by M.A. and EDX by T.W. The manuscript was written by A.K., W.B., T.H., V.V.V., and T.D. All authors discussed the results and commented on the manuscript. T.D. and T. Wojtowicz supervised the project.

-
- [1] C. W. J. Beenakker, Random-matrix theory of quantum transport, *Rev. Mod. Phys.* **69**, 731 (1997).
 - [2] A. Altland and M. R. Zirnbauer, Nonstandard symmetry classes in mesoscopic normal-superconducting hybrid structures, *Phys. Rev. B* **55**, 1142 (1997).
 - [3] S. Ryu, A. P. Schnyder, A. Furusaki, and A. W. W. Ludwig, Topological insulators and superconductors: Tenfold way and dimensional hierarchy, *New J. Phys.* **12**, 065010 (2010).
 - [4] F. Evers and A. D. Mirlin, Anderson transitions, *Rev. Mod. Phys.* **80**, 1355 (2008).
 - [5] S. Hikami, A. I. Larkin, and Y. Nagaoka, Spin-orbit interaction and magnetoresistance in the two dimensional random system, *Prog. Theor. Phys.* **63**, 707 (1980).
 - [6] T. Wojtowicz, T. Dietl, M. Sawicki, W. Plesiewicz, and J. Jaroszyński, Metal-Insulator Transition in Semimagnetic Semiconductors, *Phys. Rev. Lett.* **56**, 2419 (1986).
 - [7] A. M. Finkelstein, Electron liquid in disordered conductors, in *Soviet Scientific Reviews: Section A, Part 2*, Vol. 14, edited by I. M. Khalatnikov (Harwood Academic Publishers, Amsterdam, 1990), pp. 1–101.
 - [8] H.-Z. Lu and S.-Q. Shen, Weak localization of bulk channels in topological insulator thin films, *Phys. Rev. B* **84**, 125138 (2011).
 - [9] I. Garate and L. Glazman, Weak localization and antilocalization in topological insulator thin films with coherent bulk-surface coupling, *Phys. Rev. B* **86**, 035422 (2012).
 - [10] P. Adroguer, W. E. Liu, D. Culcer, and E. M. Hankiewicz, Conductivity corrections for topological insulators with spin-orbit impurities: Hikami-Larkin-Nagaoka formula revisited, *Phys. Rev. B* **92**, 241402(R) (2015).
 - [11] H.-W. Wang, B. Fu, and S.-Q. Shen, Anomalous Temperature Dependence of Quantum Correction to the Conductivity of Magnetic Topological Insulators, *Phys. Rev. Lett.* **124**, 206603 (2020).
 - [12] L. E. Golub, I. V. Gornyi, and V. Yu. Kachorovskii, Weak antilocalization in two-dimensional systems with large Rashba splitting, *Phys. Rev. B* **93**, 245306 (2016).
 - [13] S. Chatterjee, S. Khalid, H. S. Inbar, A. Goswami, F. C. de Lima, A. Sharan, F. P. Sabino, T. L. Brown-Heft, Y.-H. Chang, A. V. Fedorov, D. Read, A. Janotti, and C. J. Palmström, Weak antilocalization in quasi-two-dimensional electronic states of epitaxial LuSb thin films, *Phys. Rev. B* **99**, 125134 (2019).
 - [14] X. Wu, X. Li, Z. Song, C. Berger, and W. A. de Heer, Weak Antilocalization in Epitaxial Graphene: Evidence for Chiral Electrons, *Phys. Rev. Lett.* **98**, 136801 (2007).
 - [15] E. McCann, K. Kechedzhi, V. I. Fal'ko, H. Suzuura, T. Ando, and B. L. Altshuler, Weak-Localization Magnetoresistance and Valley Symmetry in Graphene, *Phys. Rev. Lett.* **97**, 146805 (2006).
 - [16] L. Fu, Topological Crystalline Insulators, *Phys. Rev. Lett.* **106**, 106802 (2011).
 - [17] C.-K. Chiu, J. C. Y. Teo, A. P. Schnyder, and S. Ryu, Classification of topological quantum matter with symmetries, *Rev. Mod. Phys.* **88**, 035005 (2016).
 - [18] T. H. Hsieh, H. Lin, J. Liu, W. Duan, A. Bansil, and L. Fu, Topological crystalline insulators in the SnTe material class, *Nat. Commun.* **3**, 982 (2012).
 - [19] S. Safaei, P. Kacman, and R. Buczko, Topological crystalline insulator (Pb,Sn)Te: Surface states and their spin polarization, *Phys. Rev. B* **88**, 045305 (2013).
 - [20] P. Dziawa, B. J. Kowalski, K. Dybko, R. Buczko, A. Szczerbakow, M. Szot, E. Łusakowska, T. Balasubramanian, B. M. Wojek, M. H. Berntsen, O. Tjernberg, and T. Story, Topological crystalline insulator states in $\text{Pb}_{1-x}\text{Sn}_x\text{Se}$, *Nat. Mater.* **11**, 1023 (2012).
 - [21] Y. Tanaka, Z. Ren, T. Sato, K. Nakayama, S. Souma, T. Takahashi, K. Segawa, and Y. Ando, Experimental realization of a topological crystalline insulator in SnTe, *Nat. Phys.* **8**, 800 (2012).
 - [22] S.-Y. Xu, C. Liu, N. Alidoust, M. Neupane, D. Qian, I. Belopolski, J. D. Denlinger, Y. J. Wang, L. A. Wray, H. Lin, G. Landolt, B. Slomski, J. H. Dil, A. Marcinkova, E. Morosan, Q. Gibson, R. Sankar, F. C. Chou, R. J. Cava, A. Bansil, and M. Z. Hasan, Observation of a topological crystalline insulator phase

- and topological phase transition in $\text{Pb}_{1-x}\text{Sn}_x\text{Te}$, *Nat. Commun.* **3**, 1192 (2012).
- [23] Y. Tanaka, T. Shoman, K. Nakayama, S. Souma, T. Sato, T. Takahashi, M. Novak, K. Segawa, and Y. Ando, Two types of Dirac-cone surface states on the (111) surface of the topological crystalline insulator SnTe, *Phys. Rev. B* **88**, 235126 (2013).
- [24] C. M. Polley, P. Dziawa, A. Reszka, A. Szczerbakow, R. Minikayev, J. Z. Domagala, S. Safaei, P. Kacman, R. Buczko, J. Adell, M. H. Berntsen, B. M. Wojek, O. Tjernberg, B. J. Kowalski, T. Story, and T. Balasubramanian, Observation of topological crystalline insulator surface states on (111)-oriented $\text{Pb}_{1-x}\text{Sn}_x\text{Se}$ films, *Phys. Rev. B* **89**, 075317 (2014).
- [25] W. Brzezicki, M. M. Wysockiński, and T. Hyart, Topological properties of multilayers and surface steps in the SnTe material class, *Phys. Rev. B* **100**, 121107(R) (2019).
- [26] B. A. Assaf, T. Phuphachong, V. V. Volobuev, G. Bauer, G. Springholz, L.-A. de Vaultier, and Y. Guldner, Magneto-optical determination of a topological index, *npj Quantum Mater.* **2**, 26 (2017).
- [27] G. Krizman, B. A. Assaf, T. Phuphachong, G. Bauer, G. Springholz, L. A. de Vaultier, and Y. Guldner, Dirac parameters and topological phase diagram of $\text{Pb}_{1-x}\text{Sn}_x\text{Se}$ from magnetospectroscopy, *Phys. Rev. B* **98**, 245202 (2018).
- [28] M. Liu, J. Zhang, C.-Z. Chang, Z. Zhang, X. Feng, K. Li, K. He, L. Li Wang, X. Chen, X. Dai, Z. Fang, Q.-K. Xue, X. Ma, and Y. Wang, Crossover between Weak Antilocalization and Weak Localization in a Magnetically Doped Topological Insulator, *Phys. Rev. Lett.* **108**, 036805 (2012).
- [29] V. Tkáč, K. Výborný, V. Komanický, J. Warmuth, M. Michiardi, A. S. Ngankeu, M. Vondráček, R. Tarasenko, M. Vališka, V. Stetsovych, K. Carva, I. Garate, M. Bianchi, J. Wiebe, V. Holý, Ph. Hofmann, G. Springholz, V. Sechovský, and J. Honolka, Influence of an Anomalous Temperature Dependence of the Phase Coherence Length on the Conductivity of Magnetic Topological Insulators, *Phys. Rev. Lett.* **123**, 036406 (2019).
- [30] M. Sawicki, T. Dietl, J. Kossut, J. Igalson, T. Wojtowicz, and W. Plesiewicz, Influence of S-D Exchange Interaction on the Conductivity of $\text{Cd}_{1-x}\text{Mn}_x\text{Se}$:In in the Weakly Localized Regime, *Phys. Rev. Lett.* **56**, 508 (1986).
- [31] R. Adhikari, V. V. Volobuev, B. Faina, G. Springholz, and A. Bonanni, Ferromagnetic phase transition in topological crystalline insulator thin films: Interplay of anomalous Hall angle and magnetic anisotropy, *Phys. Rev. B* **100**, 134422 (2019).
- [32] B. A. Assaf, F. Katmis, P. Wei, B. Satpati, Z. Zhang, S. P. Bennett, V. G. Harris, J. S. Moodera, and D. Heiman, Quantum coherent transport in SnTe topological crystalline insulator thin films, *Appl. Phys. Lett.* **105**, 102108 (2014).
- [33] R. Akiyama, K. Fujisawa, T. Yamaguchi, R. Ishikawa, and S. Kuroda, Two-dimensional quantum transport of multivalley (111) surface state in topological crystalline insulator SnTe thin films, *Nano Res.* **9**, 490 (2015).
- [34] C. H. Yan, F. Wei, Y. Bai, F. Wang, A. Q. Zhang, S. Ma, W. Liu, and Z. D. Zhang, Structure and topological transport in Pb-doping topological crystalline insulator SnTe (001) film, *J. Mater. Sci. Technol.* **44**, 223 (2020).
- [35] J. Wang, X. Liu, C. Bunker, L. Riney, B. Qing, S. K. Bac, M. Zhukovskiy, T. Orlova, S. Rouvimov, M. Dobrowolska, J. K. Furdyna, and B. A. Assaf, Weak antilocalization beyond the fully diffusive regime in $\text{Pb}_{1-x}\text{Sn}_x\text{Se}$ topological quantum wells, *Phys. Rev. B* **102**, 155307 (2020).
- [36] M. L. Peres, H. S. Monteiro, V. A. Chitta, S. de Castro, U. A. Mengui, P. H. O. Rappl, N. F. Oliveira, E. Abramof, and D. K. Maude, Experimental investigation of spin-orbit coupling in n-type PbTe quantum wells, *J. Appl. Phys.* **115**, 093704 (2014).
- [37] V. V. Afonin, J. Bergli, Y. M. Galperin, V. L. Gurevich, and V. I. Kozub, Possible weak temperature dependence of electron dephasing, *Phys. Rev. B* **66**, 165326 (2002).
- [38] J. J. Lin and J. P. Bird, Recent experimental studies of electron dephasing in metal and semiconductor mesoscopic structures, *J. Phys.: Condens. Matter* **14**, R501 (2002).
- [39] Y. Jing, S. Huang, K. Zhang, J. Wu, Y. Guo, H. Peng, Z. Liu, and H. Q. Xu, Weak antilocalization and electron-electron interaction in coupled multiple-channel transport in a Bi_2Se_3 thin film, *Nanoscale* **8**, 1879 (2016).
- [40] S. Islam, S. Bhattacharyya, H. Nhalil, M. Banerjee, A. Richardella, A. Kandala, D. Sen, N. Samarth, S. Elizabeth, and A. Ghosh, Low-temperature saturation of phase coherence length in topological insulators, *Phys. Rev. B* **99**, 245407 (2019).
- [41] I. T. Rosen, I. Yudhistira, G. Sharma, M. Salehi, M. A. Kastner, S. Oh, S. Adam, and D. Goldhaber-Gordon, Absence of strong localization at low conductivity in the topological surface state of low-disorder Sb_2Te_3 , *Phys. Rev. B* **99**, 201101(R) (2019).
- [42] H. Nakamura, D. Huang, J. Merz, J. E. Khalaf, P. Ostrovsky, A. Yaresko, D. Samal, and H. Takagi, Robust weak antilocalization due to spin-orbital entanglement in Dirac material Sr_3SnO , *Nat. Commun.* **11**, 1161 (2020).
- [43] See Supplemental Material at <http://link.aps.org/supplemental/10.1103/PhysRevB.103.245307> for additional information on the Berry phase and conductivity calculations, structural characterization and electrical properties of the epilayers, fitting of the data with the full HLN formula, phase coherence length in various topological systems, and fitting of the magnetoresistance for the in-plane magnetic field, which includes Refs. [38,62–107].
- [44] P. Wenk and S. Kettmann, Dimensional dependence of weak localization corrections and spin relaxation in quantum wires with Rashba spin-orbit coupling, *Phys. Rev. B* **81**, 125309 (2010).
- [45] B. M. Wojek, R. Buczko, S. Safaei, P. Dziawa, B. J. Kowalski, M. H. Berntsen, T. Balasubramanian, M. Leandersson, A. Szczerbakow, P. Kacman, T. Story, and O. Tjernberg, Spin-polarized (001) surface states of the topological crystalline insulator $\text{Pb}_{0.73}\text{Sn}_{0.27}\text{Se}$, *Phys. Rev. B* **87**, 115106 (2013).
- [46] S.-Y. Xu, M. Neupane, I. Belopolski, C. Liu, N. Alidoust, G. Bian, S. Jia, G. Landolt, B. Slomski, J. H. Dil, P. P. Shibayev, S. Basak, T.-R. Chang, H.-T. Jeng, R. J. Cava, H. Lin, A. Bansil, and M. Z. Hasan, Unconventional transformation of spin Dirac phase across a topological quantum phase transition, *Nat. Commun.* **6**, 6870 (2015).
- [47] H. Preier, Recent advances in lead-chalcogenide diode lasers, *Appl. Phys.* **20**, 189 (1979).
- [48] V. V. Volobuev, P. S. Mandal, M. Galicka, O. Caha, J. Sánchez-Barriga, D. Di Sante, A. Varykhalov, A. Khiar, S. Picozzi, G. Bauer, P. Kacman, R. Buczko, O. Rader, and G. Springholz, Giant Rashba splitting in $\text{Pb}_{1-x}\text{Sn}_x\text{Te}$ (111) topological crys-

- talline insulator films controlled by Bi doping in the bulk, *Adv. Mater.* **29**, 1604185 (2017).
- [49] P. S. Mandal, G. Springholz, V. V. Volobuev, O. Caha, A. Varykhalov, E. Golias, G. Bauer, O. Rader, and J. Sánchez-Barriga, Topological quantum phase transition from mirror to time reversal symmetry protected topological insulator, *Nat. Commun.* **8**, 968 (2017).
- [50] B. A. Assaf, T. Phuphachong, E. Kampert, V. V. Volobuev, P. S. Mandal, J. Sánchez-Barriga, O. Rader, G. Bauer, G. Springholz, L. A. de Vaultier, and Y. Guldner, Negative Longitudinal Magnetoresistance from the Anomalous $N = 0$ Landau Level in Topological Materials, *Phys. Rev. Lett.* **119**, 106602 (2017).
- [51] K. A. Kolwas, G. Grabecki, S. Trushkin, J. Wróbel, M. Aleszkiewicz, Ł. Cywiński, T. Dietl, G. Springholz, and G. Bauer, Absence of nonlocal resistance in microstructures of PbTe quantum wells, *Phys. Status Solidi (b)* **250**, 37 (2013).
- [52] N. Ramakrishnan, Y. T. Lai, S. Lara, M. M. Parish, and S. Adam, Equivalence of effective medium and random resistor network models for disorder-induced unsaturating linear magnetoresistance, *Phys. Rev. B* **96**, 224203 (2017).
- [53] H. Fukuyama, Non-metallic behaviors of two-dimensional metals and effect of intervalley impurity scattering, *Prog. Theor. Phys. Suppl.* **69**, 220 (1980).
- [54] S. Maekawa and H. Fukuyama, Magnetoresistance in two-dimensional disordered systems: Effects of Zeeman splitting and spin-orbit scattering, *J. Phys. Soc. Jpn.* **50**, 2516 (1981).
- [55] H.-Z. Lu, J. Shi, and S.-Q. Shen, Competition between Weak Localization and Antilocalization in Topological Surface States, *Phys. Rev. Lett.* **107**, 076801 (2011).
- [56] B. L. Al'tshuler and A. G. Aronov, Magnetoresistance of thin films and of wires in a longitudinal magnetic field, *Pisma Zh. Eksp. Teor. Fiz.* **33**, 515 (1981) [*JETP Lett.* **33**, 499 (1981)].
- [57] V. K. Dugaev and D. E. Khmel'nitskii, Magnetoresistance of metal films with low impurity concentrations in a parallel magnetic field, *Zh. Eksp. Teor. Fiz.* **86**, 1784 (1984) [*Sov. Phys. JETP* **59**, 1038 (1984)].
- [58] C. W. J. Beenakker and H. van Houten, Boundary scattering and weak localization of electrons in a magnetic field, *Phys. Rev. B* **38**, 3232 (1988).
- [59] G. Bauer, H. Pascher, and W. Zawadzki, Magneto-optical properties of semimagnetic lead chalcogenides, *Semicond. Sci. Technol.* **7**, 703 (1992).
- [60] A. G. Mal'shukov, K. A. Chao, and M. Willander, Magnetoresistance of a weakly disordered III-V semiconductor quantum well in a magnetic field parallel to interfaces, *Phys. Rev. B* **56**, 6436 (1997).
- [61] M. M. Glazov and L. E. Golub, Spin-orbit interaction and weak localization in heterostructures, *Semicond. Sci. Technol.* **24**, 064007 (2009).
- [62] A. Del Maestro, T. Hyart, and B. Rosenow, Backscattering between helical edge states via dynamic nuclear polarization, *Phys. Rev. B* **87**, 165440 (2013).
- [63] D. I. Pikulin and T. Hyart, Interplay of Exciton Condensation and the Quantum Spin Hall Effect in InAs/GaSb Bilayers, *Phys. Rev. Lett.* **112**, 176403 (2014).
- [64] J. Wang, Y. Meir, and Y. Gefen, Spontaneous Breakdown of Topological Protection in Two Dimensions, *Phys. Rev. Lett.* **118**, 046801 (2017).
- [65] F. Xue and A. H. MacDonald, Time-Reversal Symmetry-Breaking Nematic Insulators Near Quantum Spin Hall Phase Transitions, *Phys. Rev. Lett.* **120**, 186802 (2018).
- [66] J. I. Väyrynen, M. Goldstein, Y. Gefen, and L. I. Glazman, Resistance of helical edges formed in a semiconductor heterostructure, *Phys. Rev. B* **90**, 115309 (2014).
- [67] S. V. Iordanskii, Yu. B. Lyanda-Geller, and G. E. Pikus, Magnetoresistance of thin films and of wires in a longitudinal magnetic field, *Pisma Zh. Eksp. Teor. Fiz.* **60**, 199 (1994) [*JETP Lett.* **60**, 206 (1994)].
- [68] W. Knap, C. Skierbiszewski, A. Zduniak, E. Litwin-Staszewska, D. Bertho, F. Kobbi, J. L. Robert, G. E. Pikus, F. G. Pikus, S. V. Iordanskii, V. Mosser, K. Zekentes, and Yu. B. Lyanda-Geller, Weak antilocalization and spin precession in quantum wells, *Phys. Rev. B* **53**, 3912 (1996).
- [69] L. Zhao, J. Wang, B.-L. Gu, and W. Duan, Tuning surface Dirac valleys by strain in topological crystalline insulators, *Phys. Rev. B* **91**, 195320 (2015).
- [70] BaF₂ thermal expansion: Datasheet from PAULING FILE Multinaries Edition—2012, part of Springer Materials.
- [71] Lead selenide (PbSe) crystal structure, lattice parameters, thermal expansion: Datasheet from Landolt-Börnstein - Group III Condensed Matter, Volume 41C: Non-Tetrahedrally Bonded Elements and Binary Compounds I (1998), part of Springer Materials.
- [72] P. J. McCann, J. Fuchs, Z. Feit, and C. G. Fonstad, Phase equilibria and liquid-phase-epitaxy growth of PbSnSeTe lattice-matched to PbSe, *J. Appl. Phys.* **62**, 2994 (1987).
- [73] B. Tranta and H. Clemens, Epitaxial growth of PbTe doping superlattices on (111) BaF₂ and (100) GaAs, in *New Developments in Semiconductor Physics*, edited by G. Ferenczi and F. Beleznyay (Springer, Berlin, 1988), Vol. 301, pp. 281.
- [74] M. M. Parish and P. B. Littlewood, Classical magnetotransport of inhomogeneous conductors, *Phys. Rev. B* **72**, 094417 (2005).
- [75] J. Ping, I. Yudhistira, N. Ramakrishnan, S. Cho, S. Adam, and M. S. Fuhrer, Disorder-Induced Magnetoresistance in a Two-Dimensional Electron System, *Phys. Rev. Lett.* **113**, 047206 (2014).
- [76] S. Cho and M. S. Fuhrer, Charge transport and inhomogeneity near the minimum conductivity point in graphene, *Phys. Rev. B* **77**, 081402(R) (2008).
- [77] J. Hu, M. M. Parish, and T. F. Rosenbaum, Nonsaturating magnetoresistance of inhomogeneous conductors: Comparison of experiment and simulation, *Phys. Rev. B* **75**, 214203 (2007).
- [78] L. E. Golub, Weak antilocalization in high-mobility two-dimensional systems, *Phys. Rev. B* **71**, 235310 (2005).
- [79] M. O. Nestoklon, N. S. Averkiev, and S. A. Tarasenko, Weak localization of two-dimensional Dirac fermions beyond the diffusion regime, *Solid State Commun.* **151**, 1550 (2011).
- [80] Y. S. Kim, M. Brahlek, N. Bansal, E. Edrey, G. A. Kapilevich, K. Iida, M. Tanimura, Y. Horibe, S.-W. Cheong, and S. Oh, Thickness-dependent bulk properties and weak antilocalization effect in topological insulator Bi₂Se₃, *Phys. Rev. B* **84**, 073109 (2011).
- [81] L. Bao, L. He, N. Meyer, X. Kou, P. Zhang, Z. g. Chen, A. V. Fedorov, J. Zou, T. M. Riedemann, T. A. Lograsso, K. L. Wang, G. Tuttle, and F. Xiu, Weak anti-localization and quantum oscillations of surface states in topological insulator Bi₂Se₂Te, *Sci. Rep.* **2**, 726 (2012).

- [82] N. Bansal, Y. S. Kim, M. Brahlek, E. Edrey, and S. Oh, Thickness-Independent Transport Channels in Topological Insulator Bi_2Se_3 thin Films, *Phys. Rev. Lett.* **109**, 116804 (2012).
- [83] B. A. Assaf, T. Cardinal, P. Wei, F. Katmis, J. S. Moodera, and D. Heiman, Linear magnetoresistance in topological insulator thin films: Quantum phase coherence effects at high temperatures, *Appl. Phys. Lett.* **102**, 012102 (2013).
- [84] J. Lee, J. Park, J.-H. Lee, J. S. Kim, and H.-J. Lee, Gate-tuned differentiation of surface-conducting states in $\text{Bi}_{1.5}\text{Sb}_{0.5}\text{Te}_{1.7}\text{Se}_{1.3}$ topological-insulator thin crystals, *Phys. Rev. B* **86**, 245321 (2012).
- [85] S.-P. Chiu and J.-J. Lin, Weak antilocalization in topological insulator Bi_2Te_3 microflakes, *Phys. Rev. B* **87**, 035122 (2013).
- [86] A. A. Taskin, S. Sasaki, K. Segawa, and Y. Ando, Achieving surface quantum oscillations in topological insulator thin films of Bi_2Se_3 , *Adv. Mater.* **24**, 5581 (2012).
- [87] C. Shekhar, C. E. ViolBarbosa, B. Yan, S. Ouardi, W. Schnelle, G. H. Fecher, and C. Felser, Evidence of surface transport and weak antilocalization in a single crystal of the $\text{Bi}_2\text{Te}_2\text{Se}$ topological insulator, *Phys. Rev. B* **90**, 165140 (2014).
- [88] Y. Pan, D. Wu, J. R. Angevaere, H. Luigjes, E. Frantzeskakis, N. de Jong, E. van Heumen, T. V. Bay, B. Zwartsenberg, Y. K. Huang, M. Snelder, A. Brinkman, M. S. Golden, and A. de Visser, Low carrier concentration crystals of the topological insulator $\text{Bi}_{2-x}\text{Sb}_x\text{Te}_{3-y}\text{Se}_y$: A magnetotransport study, *New J. Phys.* **16**, 123035 (2014).
- [89] W. J. Wang, K. H. Gao, and Z. Q. Li, Thickness-dependent transport channels in topological insulator Bi_2Se_3 thin films grown by magnetron sputtering, *Sci. Rep.* **6**, 25291 (2016).
- [90] K. Banerjee, J. Son, P. Deorani, P. Ren, L. Wang, and H. Yang, Defect-induced negative magnetoresistance and surface state robustness in the topological insulator BiSbTeSe_2 , *Phys. Rev. B* **90**, 235427 (2014).
- [91] R. K. Gopal, S. Singh, R. Chandra, and C. Mitra, Weak-antilocalization and surface dominated transport in topological insulator $\text{Bi}_2\text{Se}_2\text{Te}$, *AIP Adv.* **5**, 047111 (2015).
- [92] P. Ngabonziza, M. P. Stehno, H. Myoren, V. A. Neumann, G. Koster, and A. Brinkman, Gate-tunable transport properties of in situ capped Bi_2Te_3 topological insulator thin films, *Adv. Electron. Mater.* **2**, 1600157 (2016).
- [93] M. Zhang, Z. Wei, R. Jin, Y. Ji, Y. Yan, X. Pu, X. Yang, and Y. Zhao, Electrical transport properties and morphology of topological insulator Bi_2Se_3 thin films with different thickness prepared by magnetron sputtering, *Thin Solid Films* **603**, 289 (2016).
- [94] B. A. Assaf, T. Cardinal, P. Wei, F. Katmis, J. S. Moodera, and D. Heiman, Modified electrical transport probe design for standard magnetometer, *Rev. Sci. Instrum.* **83**, 033904 (2012).
- [95] C. Zhang, Y. Liu, X. Yuan, W. Wang, S. Liang, and F. Xiu, Highly tunable Berry phase and ambipolar field effect in topological crystalline insulator $\text{Pb}_{1-x}\text{Sn}_x\text{Se}$, *Nano Lett.* **15**, 2161 (2015).
- [96] R. Zhong, X. He, J. A. Schneeloch, C. Zhang, T. Liu, I. Pletikosić, T. Yilmaz, B. Sinkovic, Q. Li, W. Ku, T. Valla, J. M. Tranquada, and G. Gu, Surface-state-dominated transport in crystals of the topological crystalline insulator In-doped $\text{Pb}_{1-x}\text{Sn}_x\text{Te}$, *Phys. Rev. B* **91**, 195321 (2015).
- [97] A. Zhang, F. Wei, C. Yan, F. Wang, S. Ma, and Z. Zhang, Topological phase transition and highly tunable topological transport in topological crystalline insulator $\text{Pb}_{1-x}\text{Sn}_x\text{Te}$ (111) thin films, *Nanotechnology* **30**, 275703 (2019).
- [98] K. Zou, S. D. Albright, O. E. Dagdeviren, M. D. Morales-Acosta, G. H. Simon, C. Zhou, S. Mandal, S. Ismail-Beigi, U. D. Schwarz, E. I. Altman, F. J. Walker, and C. H. Ahn, Revealing surface-state transport in ultrathin topological crystalline insulator SnTe films, *APL Mater.* **7**, 051106 (2019).
- [99] K. Dybko, G. P. Mazur, W. Wolkanowicz, M. Szot, P. Dziawa, J. Z. Domagala, M. Wiater, T. Wojtowicz, G. Grabecki, and T. Story, Probing spatial extent of topological surface states by weak antilocalization experiments, [arXiv:1812.08711](https://arxiv.org/abs/1812.08711).
- [100] B. L. Altshuler, A. G. Aronov, and D. E. Khmel'nitsky, Effects of electron-electron collisions with small energy transfers on quantum localisation, *J. Phys. C: Solid State Phys.* **15**, 7367 (1982).
- [101] S. Datta, *Electronic Transport in Mesoscopic Systems* (Cambridge University Press, Cambridge, 1995).
- [102] A. Prinz, G. Brunthaler, Y. Ueta, G. Springholz, G. Bauer, G. Grabecki, and T. Dietl, Electron localization in $n\text{-Pb}_{1-x}\text{Eu}_x\text{Te}$, *Phys. Rev. B* **59**, 12983 (1999).
- [103] G. Tkachov and E. M. Hankiewicz, Weak antilocalization in HgTe quantum wells and topological surface states: Massive versus massless Dirac fermions, *Phys. Rev. B* **84**, 035444 (2011).
- [104] G. Tkachov and E. M. Hankiewicz, Spin-helical transport in normal and superconducting topological insulators, *Phys. Status Solidi (b)* **250**, 215 (2013).
- [105] H. Mathur and H. U. Baranger, Random Berry phase magnetoresistance as a probe of interface roughness in Si MOSFET's, *Phys. Rev. B* **64**, 235325 (2001).
- [106] G. M. Minkov, O. E. Rut, A. V. Germanenko, A. A. Sherstobitov, B. N. Zvonkov, V. I. Shashkin, O. I. Khrykin, and D. O. Filatov, Transverse negative magnetoresistance of two-dimensional structures in the presence of a strong in-plane magnetic field: Weak localization as a probe of interface roughness, *Phys. Rev. B* **70**, 035304 (2004).
- [107] C. J. Lin, X. Y. He, J. Liao, X. X. Wang, V. Sacksteder IV, W. M. Yang, T. Guan, Q. M. Zhang, L. Gu, G. Y. Zhang, C. G. Zeng, X. Dai, K. H. Wu, and Y. Q. Li, Parallel field magnetoresistance in topological insulator thin films, *Phys. Rev. B* **88**, 041307(R) (2013).